Supporting Information

Synergetic and persistent harvest of electricity and potable water from ambient moisture with biohybrid fibrils

*Xiao Han[†, §], Weihua Zhang[‡], Xinpeng Che[†, §], Lifen Long[#], Mingjie Li[†, §, *] and Chaoxu Li[†, §, *]*

[†]Group of Biomimetic Smart Materials, Qingdao Institute of Bioenergy and Bioprocess Technology, Chinese Academy of Sciences & Shandong Energy Institute, Songling Road 189, Qingdao 266101, P. R. China

[§]Center of Material and Optoelectronics Engineering, University of Chinese Academy of Sciences, 19A Yuquan Road, Beijing 100049, P. R. China

[‡]Johan Gadolin Process Chemistry Centre, c/o Laboratory of Wood and Paper Chemistry, Åbo Akademi University, Turku FI-20500, Finland

[#]WEEE Research Centre, Research Center of Resource Recycling Science and Engineering, Shanghai Polytechnic University, Shanghai Collaborative Innovation Centre for WEEE Recycling, Shanghai 201209, P. R. China

*Corresponding authors: Chaoxu Li (Email: licx@qibebt.ac.cn); Mingjie Li (Email: limj@qibebt.ac.cn)

Table of contents in Supporting Information:

EXPERIMENTAL SECTION

Synthesis of biological fibrils could be found in our previous works[S1]. Carboxyl cellulose fibrils (with the diameter ~6 nm, aspect ratio >10^3 and carboxyl content ~1.2 mmol g^{-1}); Deacetylated chitin nanocrystals (diameter ~14 nm, aspect ratio >10^2, deacetylation degree ~17.5%); NaClO-oxidized silk fibrils (diameter ~11 nm, aspect ratio >10^2).

Ni^{2+}-exchanged sulfonated cellulose fibrils.[S2] A solution of $Ni(NO_3)_2 \cdot 6H_2O$ with excessive Ni^{2+} was added to the sulfonated cellulose fibrils suspension with a concentration of 0.5 mg mL^{-1} and the mixture was stirred for 2 h. The suspension was then centrifuged and washed with pure water, and redispersed into water for a desired concentration.

Synthesis of MOF powder. The pure $Ni_2(HHTP)_3$ and $Ni_2(HITP)_3$ powders were synthesized by a solvothermal method. In typical, an aqueous solution of $Ni(OAc)_2 \cdot 4H_2O$ (60 mg) in 10 mL water was added to another aqueous solution of HHTP (42 mg) in 10 mL water. The solution was stirred at 80 °C for 12 h. The resultant blue dark powders were washed and immersed in acetone for 1 week, and then collected and dried at 70 °C for 12 h. $Ni_2(HITP)_3$ powders were synthesized by mixing 10 mL aqueous solution of $Ni(NO_3)_2 \cdot 6H_2O$ (66 mg) and 10 mL aqueous solution (25 mL) of HITP·6HCl (100 mg). The mixture solution was stirred at 70 °C for 2 h in air and then 4 h after sealed. The obtained precipitates were collected and washed by pure water for three times, and then dried under 70 °C for 12 h.[S2]

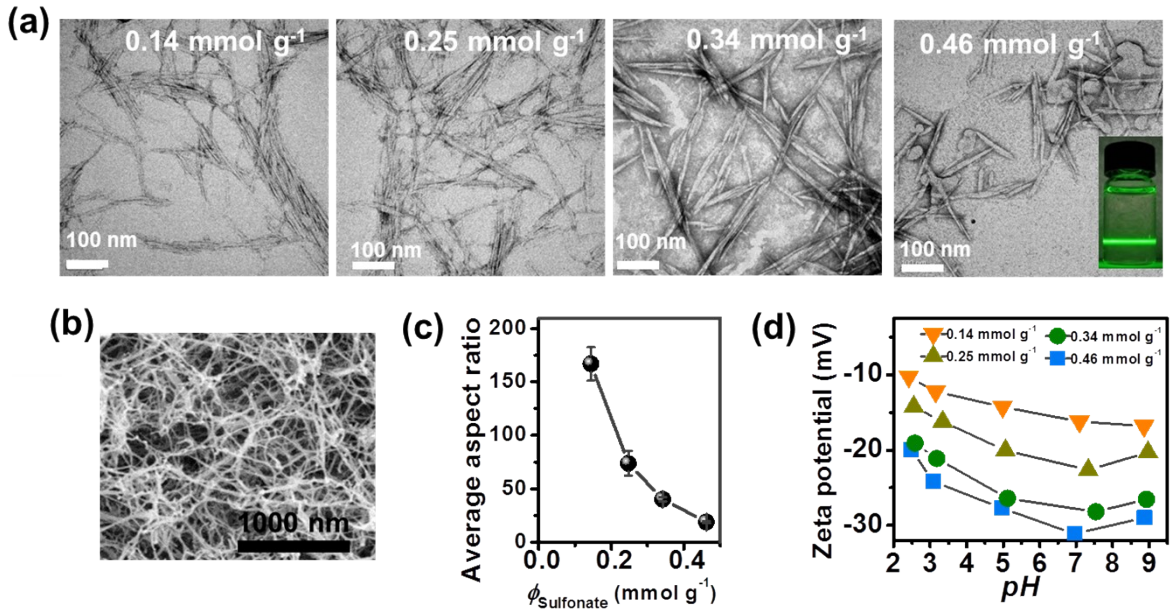

Figure S1. (a) Typical TEM images of sulfonated cellulose fibrils with different contents of sulfonate groups. Visual observation of their suspension is given as the Inset. (b) Typical SEM image of sulfonated cellulose fibrils. (c) Variation of aspect ratio with content of sulfonate groups ($\varphi_{\text{sulfonate}}$). (d) Zeta potential of sulfonate cellulose fibrils with indicated content of sulfonate groups at different pH values.

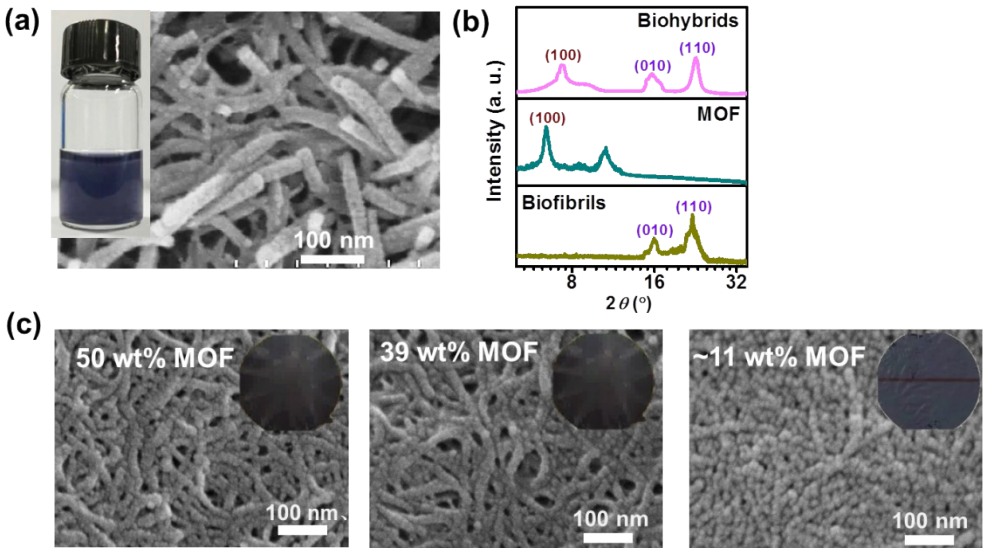

Figure S2. (a) SEM image of freeze-dried biohybrids. MOF content: 50 wt% $Ni_3(HHTP)_2$. Visual observation of their suspension is given as the Inset. (b) XRD patterns of biohybrid in comparison with pure sulfonated cellulose fibrils (as "Biofibrils") and $Ni_3(HHTP)_2$ (as "MOF"). Biohybrid fibrils had a relatively broader and weaker (100) diffraction peak than that of bulk MOF crystals of $Ni_3(HHTP)_2$. (c) SEM images and visual observation of biohybrid membranes with indicated content of $Ni_3(HHTP)_2$.

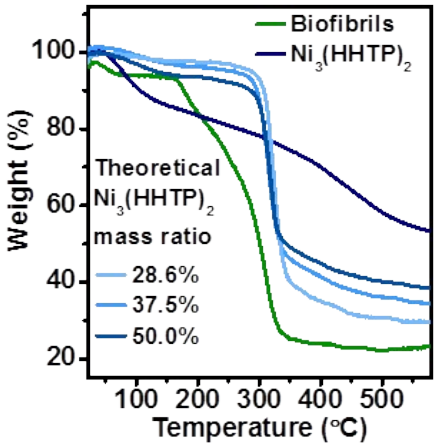

Figure S3. TG curves of biohybrids membranes with different $Ni_3(HHTP)_2$ contents.

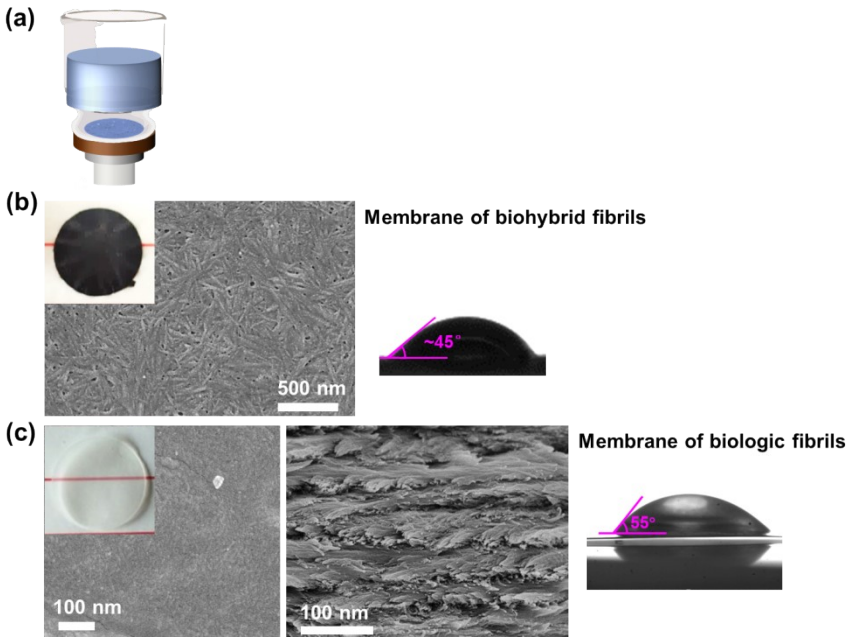

Figure S4. (a) Filtration setup for membrane production. (b) Surface SEM image, visual observation and water contact angle of biohybrids membrane. (c) Surface and cross-sectional SEM images, visual observation and water contact angle of bio-fibrils membrane.

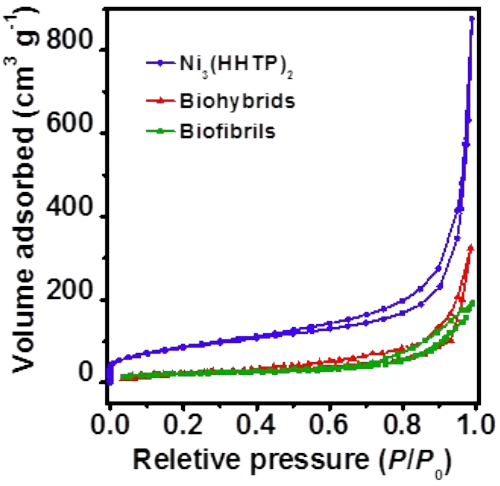

Figure S5. N_2 adsorption isotherms of biohybrids in comparison with pure biofibrils and $Ni_3(HHTP)_2$. MOF content of biohybrid: 50 wt% $Ni_3(HHTP)_2$.

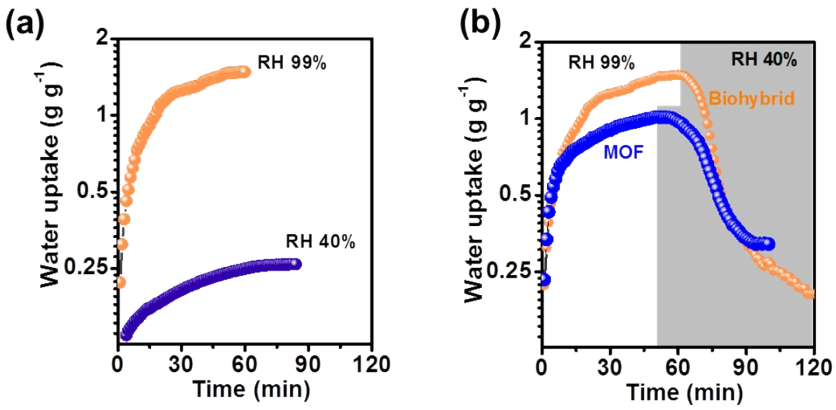

Figure S6. (a) Moisture adsorption curves of biohybrids membrane at different RH values. (b) Moisture adsorption curve at RH 99% and desorption curve at RH 40% of biohybrids membrane and $Ni_3(HHTP)_2$. MOF content of biohybrid: 50 wt% $Ni_3(HHTP)_2$. The membrane of core-shell biohybrid fibers has larger pore volume and surface area than pure biofibrils membrane. So, water uptake capacity of biohybrid is much higher than that of pure biofibrils. Capillary condensation adsorption should occur because most pores of biohybrids are larger than this critical value of 2.07 nm, in sharp contrast to the pure MOFs.

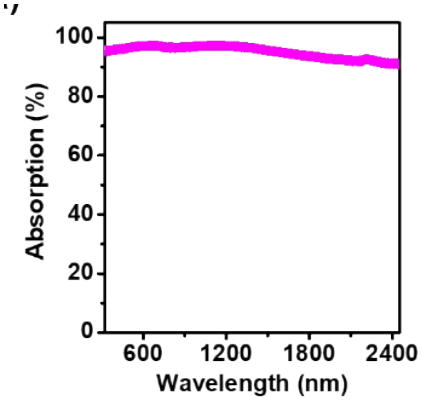

Figure S7. Ultraviolet-visible-near infrared absorption spectra for the hybrid membrane (~150 μm thick; Diffuse reflectance spectrophotometry). Ultraviolet-visible-near infrared absorption spectra have shown that the membrane of biohybrid fibrils strongly absorbs light (≥90%) throughout the solar spectrum range as a result of the highly conjugated molecular structure of the selected MOF[(S3)]. Another reason for the high temperature obtained on the membrane of biohybrid fibrils should be its ultra-low thermal conductivity (0.045 W m^{-1} K^{-1}) [(S4)].

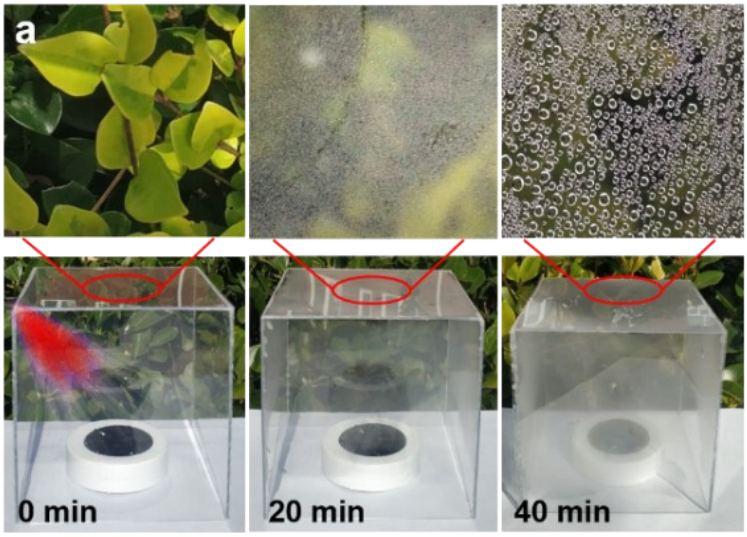

Figure S8. Visual observation of fully hydrated biohybrid membrane in transparent chamber when exposing to 1 equivalent sunlight for different periods of time. MOF content of biohybrids: 50 wt% $Ni_3(HHTP)_2$.

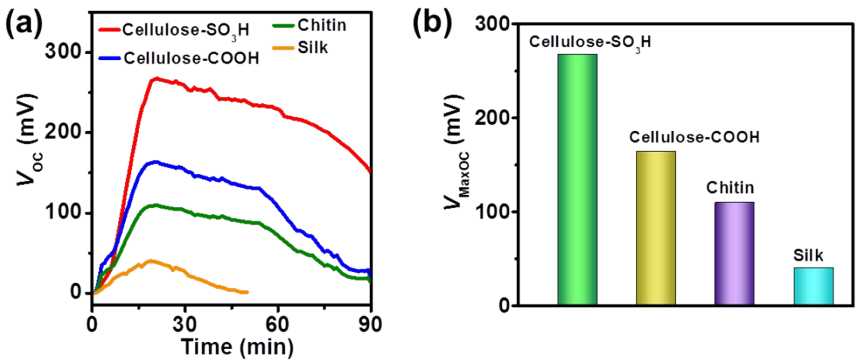

Figure S9. V_{oc} (a) and V_{MaxOC} (b) of membranes of different biologic fibrils. Membrane size: 1 × 1 cm^2. RH: 99%. Nanofibrils of sulfonated (as "Cellulose-SO_3H") and carboxyl cellulose (as "Cellulose-COOH"), deacetylated chitin (as "Chitin") and NaClO-oxidized silk (as "Silk"). According to the mechanism of harvesting electricity from ambient moisture, electricity should come from the gradient of dissociated ions and their transport[S5]. In comparison with other dissociable groups, sulfonate groups are more liable to ionize on account of their low pKa value (~1.6 in contrast to ~18 for phenolic hydroxyl and ~4 for carboxyl).[S6-S7] and thus beneficial for water adsorption and moisture-electricity generating.

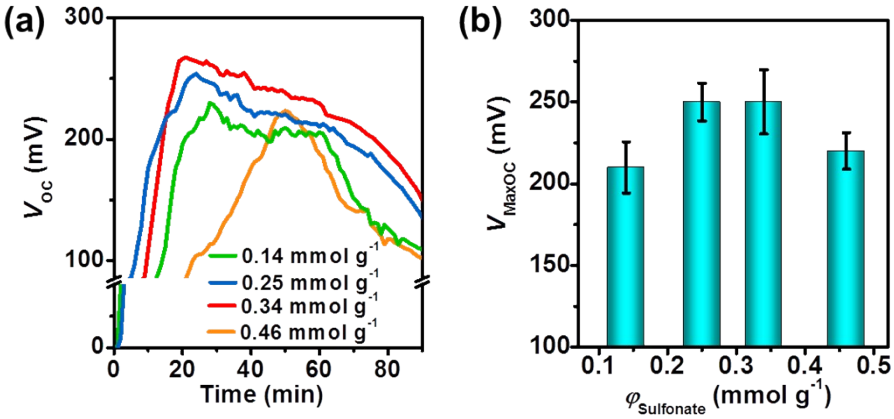

Figure S10. V_{oc} (a) and V_{MaxOC} (b) of membranes of cellulose fibrils with different $\varphi_{sulfonate}$.

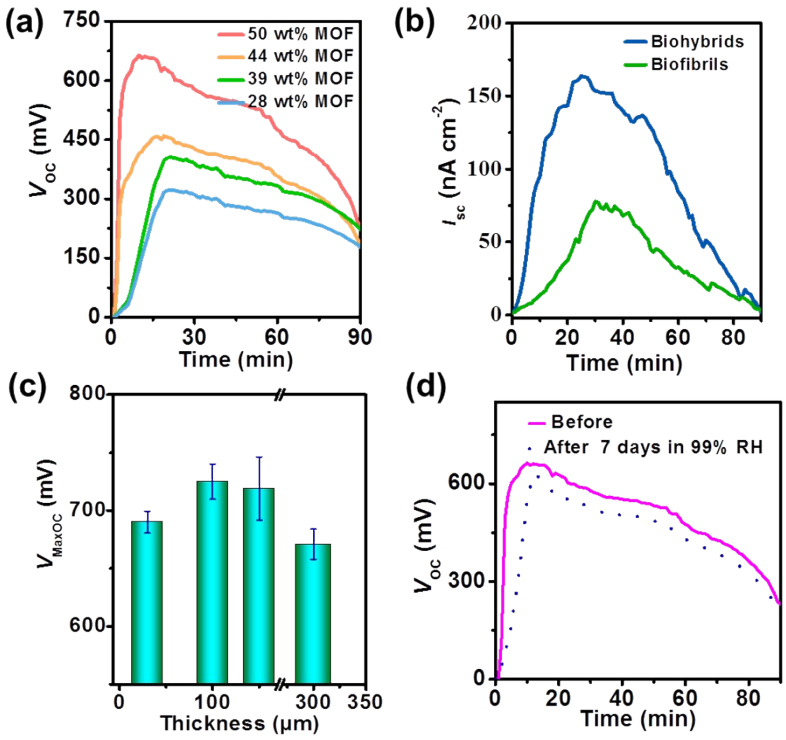

Figure S11. (a) V_{oc} variation of biohybrids membrane with different $Ni_3(HHTP)_2$ contents. (b) Short-circuit current (I_{sc}) variation of membranes of biohybrids and biofibrils. In principle[(S5)], electricity obtained in this work should come from the gradient of dissociated ions and their transport during moisture adsorption from one membrane side. Enhanced hydration from MOF coating would increase the group dissociation and thereby strengthen the electricity harvest ability. Electronic conductivity of loaded conductive MOFs might contribute to the electrical output because good conductivity can facilitate the hoping of charged carriers[(S5)]. Moreover, biohybrid fibrils have higher porosity and larger specific surface area, which would improve the accessibility of dissociable groups and thereby boost the ions dissociation and transport. (c) V_{MaxOC} of biohybrid with 50 wt% $Ni_3(HITP)_2$ at different membrane thicknesses. (d) Comparison of V_{oc} when varying RH from xx to 99% before and after incubating biohybrid membrane at 99% RH for 7 days. MOF content of biohybrids: 50 wt% $Ni_3(HHTP)_2$.

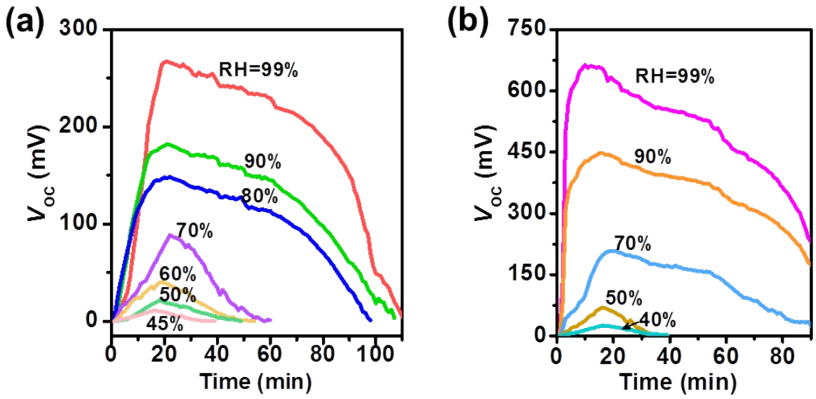

Figure S12. Temporal V_{oc} variation of membranes of biofibrils (a) and biohybrids (b) when varying RH from 35% to indicated values. MOF content of biohybrids: 50 wt% $Ni_3(HHTP)_2$.

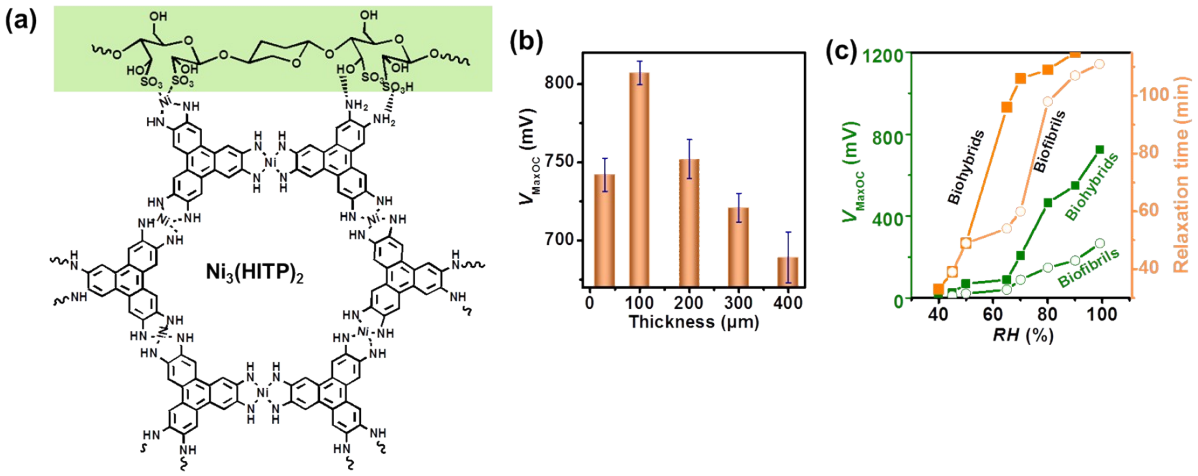

Figure S13. (a) Schematic illustration of interactions between $Ni_3(HITP)_2$ and sulfonate cellulose fibrils. (b) V_{MaxOC} of biohybrid membrane when varying RH from 35% to 99%. (c) V_{MaxOC} and relaxation time variation of biohybrid membrane when varying RH from 35% to 99%. MOF content of biohybrids: 50 wt% $Ni_3(HITP)_2$.

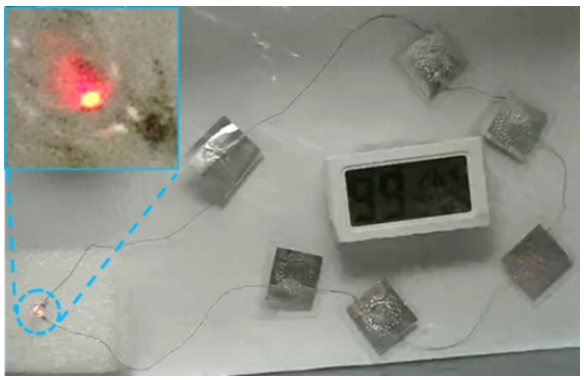

Figure S14. Visual observation of unit devices in series to light a red LED.

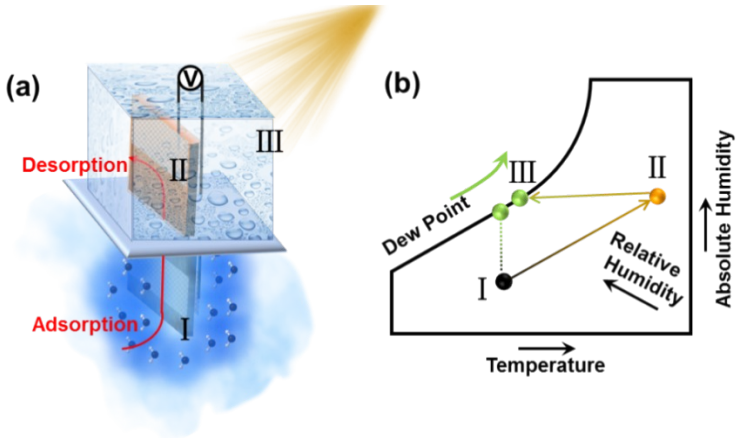

Figure S15. Schematic illustration of the process of synergetic and persistent harvest of electricity and potable water from air moisture: The setup (a) coupled with psychrometric chart (b). Water molecules in the atmosphere are, firstly, adsorbed by the bottom part of the biohybrid membrane (marked as state I). RH difference would transport water up to the top of the biohybrid membrane (marked as state II). Persistent sunlight irradiation would increase the temperature of the top part, desorb water into the air and decrease the RH at state II. When RH at state I is higher than that at state II, persistent water adsorption at bottom part and water desorption at top part could be realized coupled with the persistent water transport from the bottom to the top. This continuous electricity generation should be probabily from streaming potential. When the desobed water molecules reach at the wall of the system whose temperature is lower than the dew point, water molecules would condense into potable water droplets (marked as state III). This dynamic equilibrium process enabled the synergetic and persistent harvest of electricity and potable water from air moisture.

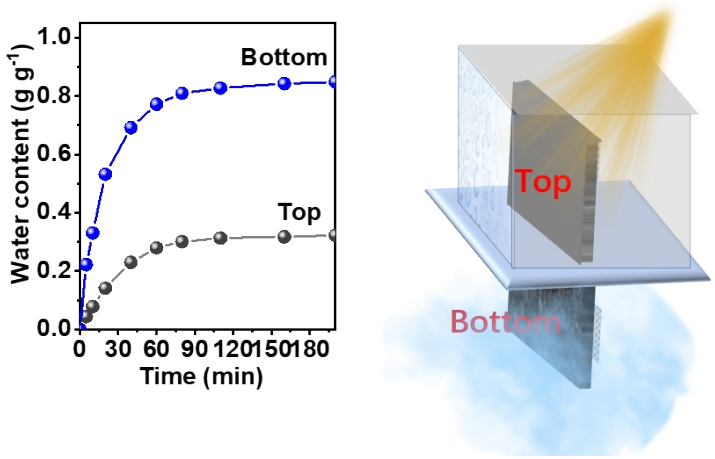

Figure S16. Comparison of water content of Top part of biohybrid membrane with Bottom part. Top part is exposing to one equivalent sunlight. Bottom part is exposing to RH ~99%. The lower water content value of Top part is resulted from photo-thermal effect of biohybrid. MOF content of biohybrids: 50 wt% $Ni_3(HHTP)_2$. Membrane size: 1 × 5 cm^2. Membrane thickness: 100 μm. In this test, many sets of experiments were carried out for different time periods. At one pre-set time, some membranes were cut in the middle to form the upper part and the lower part. After weighed respectively by an electronic balance (ME204E, Mettler Toledo, Switzerland), the upper and the lower part were fully desorbed at 100 °C and RH 35% until to get a constant weight. The moisture uptake at that time was evaluated through the weight variation. And at other pre-set times, other sets of membranes were undergone the similar processes.

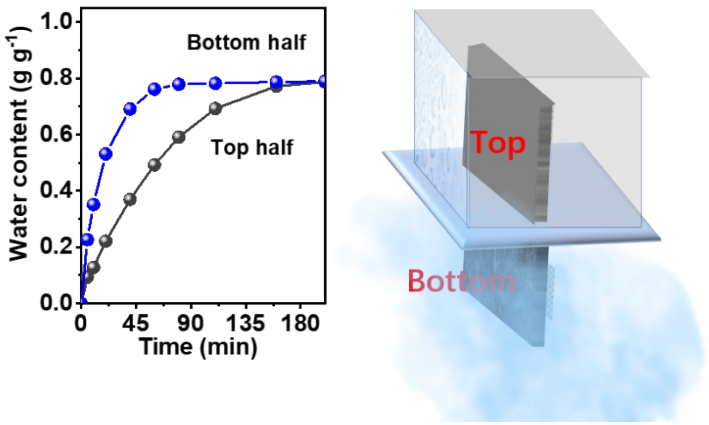

Figure S17. Comparison of water content of Top part of biohybrid membrane with Bottom part. Bottom part is exposing to RH ~99%. MOF content of biohybrids: 50 wt% $Ni_3(HHTP)_2$. Membrane size: 1 × 5 cm^2. Membrane thickness: 100 μm. Because ambient air is of saturated humidity capillary condensation should occur during moisture adsorption within the lower part. The water transport from lower part to the upper part may include molecular diffusion driven by RH difference and fluidic permeability driven by capillary force. When moisture adsorption was balanced by photo-thermal desorption, synergetic and persistent harvest of electricity and water was achieved.

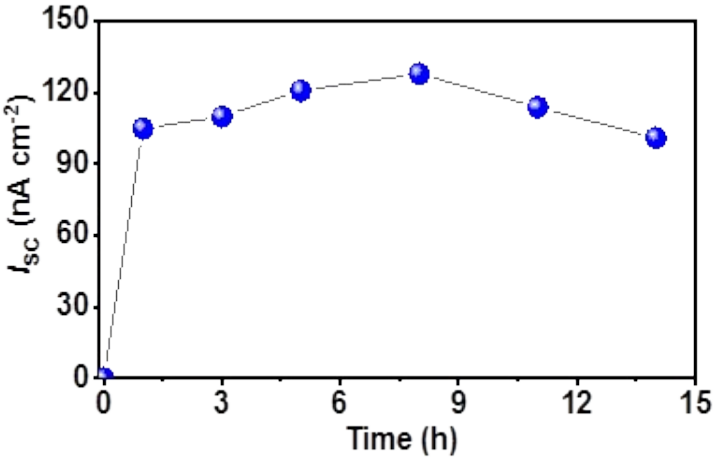

Figure S18. Temporal variation of I_{sc} during long-term harvesting electricity and water from ambient moisture. RH ~99%. MOF content of biohybrids: 50 wt% $Ni_3(HHTP)_2$. Membrane size: 1 × 5 cm^2. Membrane thickness: 100 μm.

Supporting tables

Table S1 Moisture adsorption performance of hybrid fibrils compared with typical reported MOF materials.

Sample	Capacity ($g\ g^{-1}$)	Time used (min)	Conditions (RH/%;temperature/°C)	Reference
Cr-MIL-101 powder	1.25	950	70; 35	(S8)
Ti-MIL-125	0.41	100	70; 35	(S8)
Zr-MOF-808	0.74	50	70; 22	(S8)
Ti-MIL-125-NH_2	0.22	60	70; 22	(S8)
Zr-UiO-66-NH_2	0.35	60	70; 22	(S8)
MOF-303	0.41	100	40; 30	(S9)
SAPO-34	0.30	80	40; 30	(S9)
Al-fumarate	0.29	50	40; 30	(S9)
Zeolite-13X	0.39	150	40; 30	(S9)
	1.48	60	99; 20	
	0.98	68	80; 20	
Biohybrid fibrils	0.61	80	60; 20	This work
	0.36	120	50; 20	
	0.96	50	99; 40	

Supporting References

(S1) Li, M.; Zong, L.; Yang, W.; Li, X.; You, J.; Wu, X.; Li, Z.; Li, C. Biological Nanofibrous Generator for Electricity Harvest from Moist Air Flow. *Adv. Funct. Mater.* **2019,** *29*, 1901798.

(S2) Zhou, S.; Kong, X.; Zheng, B.; Huo, F.; Strømme, M.; Xu, C. Cellulose Nanofiber@Conductive Metal–Organic Frameworks for High-Performance Flexible Supercapacitors. *ACS Nano* **2019,** *13*, 9578-9586.

(S3) Sheberla, D.; Sun, L.; Blood-Forsythe, M. A.; Er, S.; Wade, C. R.; Brozek, C. K.; Aspuru-Guzik, A.; Dincă, M. High Electrical Conductivity in Ni_3(2,3,6,7,10,11-hexaiminotriphenylene)$_2$, a Semiconducting Metal-Organic Graphene Analogue. *J. Am. Chem. Soc.* **2014,** *136*, 8859-8862.

(S4) Zhou, S.; Qiu, Z.; Strømme, M.; Xu, C. Solar-Driven Ionic Power Generation via a Film of Nanocellulose@Conductive Metal-Organic Framework. *Energy Environ. Sci.* **2021,** *14*, 900-905.

(S5) Shen, D.; Duley, W.; Peng, P.; Xiao, M.; Zhou, Y. N. Moisture Enabled Electricity Generation: From Physics and Materials to Self Powered Applications. *Adv. Mater.* **2020,** *32*, 2003722.

(S6) Bordwell, F. G.; McCallum, R. J.; Olmstead, W. N. Acidities and Hydrogen Bonding Of Phenols in Dimethyl Sulfoxide. *J. Org. Chem.* **1984,** *49*, 1424-1427.

(S7) Braude, E. A.; Nachod, F. C. *Determination of Organic Structures by Physical Methods*. Elsevier: New York, 1971.

(S8) Logan, M. W.; Langevin, S.; Xia, Z. Reversible Atmospheric Water Harvesting Using Metal-Organic Frameworks. *Sci. Rep.* **2020,** *10*, 1492.

(S9) Hanikel, N.; Prévot, M. S.; Fathieh, F.; Kapustin, E. A.; Lyu, H.; Wang, H.; Diercks, N. J.; Glover, T. G.; Yaghi, O. M. Rapid Cycling and Exceptional Yield in a Metal-Organic Framework Water Harvester. *ACS central science* **2019,** *5*, 1699-1706.